Structure and magnetic properties of $R\mathrm{Fe}_{11.35}\mathrm{Nb}_{0.65}$ and $R\mathrm{Fe}_{11.35}\mathrm{Nb}_{0.65}\mathrm{N}_y$ (R = Y, Sm, Gd, Tb, Dy, Ho, Er, and Lu)

Bo-Ping Hu, Kai-Ying Wang, Yi-Zhong Wang, and Zhen-Xi Wang
San Huan Research Laboratory, Chinese Academy of Sciences, P.O. Box 603, Beijing 100080, China

Qi-Wei Yan, Pan-Lin Zhang, and Xiang-Dong Sun
Magnetism Laboratory, Institute of Physics, Chinese Academy of Sciences, P.O. Box 603, Beijing 100080, China
(Received 5 August 1994; revised manuscript received 27 September 1994)

A series of compounds with the ThMn_{12}-type structure $R\mathrm{Fe}_{11.35}\mathrm{Nb}_{0.65}$ (R = Y, Sm, Gd, Tb, Dy, Ho, Er, and Lu), were synthesized. The corresponding nitrides, obtained by gas-solid reactions, retained the same structure as their parent compounds, but with a relative volume expansion of 3%. The Nb atoms occupy the 8*i* sites in the ThMn_{12} structure. The highest Curie temperatures are 597 K and 773 K for $\mathrm{GdFe}_{11.35}\mathrm{Nb}_{0.65}$ and its nitride, respectively. The average iron magnetic moment μ_{Fe} at $T=1.5$ K is $1.9\mu_B$ for parent compounds and $2.1\mu_B$ for the nitrides. By the introduction of nitrogen, the Fe-Fe exchange interaction is much strengthened while the R-Fe exchange interaction is slightly weakened. The enhancement of μ_{Fe} by the influence of interstitial nitrogen is about 11%. The Fe sublattices of $R\mathrm{Fe}_{11.35}\mathrm{Nb}_{0.65}$ compounds and their nitrides have an easy *c*-axis anisotropy. At $T=1.5$ K, the anisotropy constant K_1(Fe) is 25.7 K/f.u. for the parent compounds and 21.9 K/f.u. for the nitrides. The reduction of K_1(Fe) by the influence of interstitial nitrogen is about 17%. Spin-reorientation transitions were observed in $\mathrm{DyFe}_{11.35}\mathrm{Nb}_{0.65}$ and $\mathrm{ErFe}_{11.35}\mathrm{Nb}_{0.65}$ compounds. The complex magnetic behavior of $R\mathrm{Fe}_{11.35}\mathrm{Nb}_{0.65}$ at low temperatures can be explained by exchange and crystal-field-interaction models. The $\mathrm{SmFe}_{11.35}\mathrm{Nb}_{0.65}$ compound has an anisotropy field of 10.0 T at room temperature. Its high Curie temperature and magnetization make it a potential candidate for applications as a permanent magnet.

I. INTRODUCTION

During the past few years, iron-rich rare-earth intermetallic compounds with the ThMn_{12} structure have been actively investigated due to their potential application as permanent magnets. The pure $R\mathrm{Fe}_{12}$ compound does not exist for any of the rare-earth atoms, but the ThMn_{12} structure can be stabilized in pseudobinaries $R\mathrm{Fe}_{12-x}M_x$, where M=Al, Ti, V, Cr, Mo, W, Si, and Re.[1–3] In these compounds, the stabilizing-element values of x are usually $1.0<x<4.0$. Among them, only the samarium compound $\mathrm{SmFe}_{12-x}M_x$ has a strong uniaxial anisotropy. By nitrogenation or carbonation, the magnetic properties of the interstitial compound $R\mathrm{Fe}_{12-x}M_xZ_y$ (Z=N or C) are greatly modified.[4–6] The interstitial nitrogen atoms not only have the effect of increasing the Curie temperature and the saturation magnetization, but they also give rise to a profound change in the magnetocrystalline anisotropy with the sign change of the second-order crystal-field coefficient. The $R\mathrm{Fe}_{12-x}M_x\mathrm{N}_y$ (R=Pr or Nd; M=Ti, V, or Mo) compounds may qualify as hard magnetic materials.[7–14]

Generally speaking, the third nonmagnetic element M has a detrimental influence on both the Curie temperature and spontaneous magnetization. Thus, for the purpose of application, the smallest possible amount of M is preferred. Very recently, the Mo content was reduced to $x=0.5$ to stabilize the $\mathrm{YFe}_{12-x}\mathrm{Mo}_x$ phase.[15] In this work, we find that $R\mathrm{Fe}_{12-x}\mathrm{Nb}_x$ members of the family of ThMn_{12}-structure compounds can be synthesized with a low Nb content of $0.5<x<0.8$. In order to improve the understanding of 1:12 compounds, we systematically investigate the phase formation, as well as the structural and intrinsic magnetic properties of $R\mathrm{Fe}_{12-x}\mathrm{Nb}_x$ and its nitride, where R=Y, Sm, Gd, Tb, Dy, Ho, Er, and Lu.

II. EXPERIMENTAL METHODS

The $R\mathrm{Fe}_{12-x}\mathrm{Nb}_x$ alloys were prepared by arc-melting 99.9% pure constituent elements with approximately 10% excess of rare-earth elements, to compensate the loss during melting. The nitrides were formed by heat-treating pulverized powder (<20 μm) in nitrogen at about 773 K for 3 h. First, we prepared $\mathrm{GdFe}_{12-x}\mathrm{Nb}_x$ compounds with $x=0.4$, 0.5, 0.65, 0.8, 1.0, 1.2, and 1.5 for the study of phase formation. Then we prepared $R\mathrm{Fe}_{12-x}\mathrm{Nb}_x$ with $x=0.65$ for R=Y, Sm, Gd, Tb, Dy, Ho, Er, Lu, and their nitrides. Attempts to prepare the compounds with rare-earth elements lighter than Sm were unsuccessful. The oriented samples for the magneto-crystalline anisotropy study were made by mixing well-ground fine powder with epoxy resin and then setting it in an applied field of 1–2 T.

Phase identification was made by powder x-ray diffraction and thermomagnetic scans at low magnetic fields. The site occupation of Nb in the ThMn_{12} structure was determined by neutron-powder diffraction.

Neutron-powder-diffraction data at room temperature were collected on the triple-axis spectrometer at the China Institute of Atomic Energy, Beijing, at a wavelength

of 1.541 Å. About 15 g of the powder sample was used and placed in a vanadium tube. The triple-axis spectrometer was used as a two-axis powder spectrometer in order to improve the resolution. The setup included a PG-Graphite monochromator (004 plane), an analyzer (002 plane), and four collimators of 30′ divergence.

The Curie temperature T_c was determined from the magnetization measured as a function of temperature using a vibrating-sample magnetometer with a steady applied field $B_0=0.04$ T. Measurements at low temperatures in a similar field were made on alloy bulk samples and on nitride powders to determine the spin-reorientation transition temperatures. An extracting-sample magnetometer and an ac susceptibility magnetometer with $f=220$ Hz and $B_0=0.1$ mT were used to obtain the measurements.

Magnetization curves of free powder or oriented samples were measured by the extracting-sample magnetometer and by a pulse-field instrument. The saturation magnetization M_s was obtained by extrapolating $M-1/B_0^2$ to $1/B_0^2\rightarrow 0$.

The anisotropy field B_a was determined by a singular point detection (SPD) technique[16] on a pulse-field system up to the applied field of 10 T or by magnetization measurements along and perpendicular to the alignment direction on the oriented samples.

In addition, the alloy composition was checked by inductively coupled plasma (ICP).

III. RESULTS AND DISCUSSIONS

A. $ThMn_{12}$-structure phase formation in Gd-Fe-Nb alloys

A series of $GdFe_{12-x}Nb_x$ alloys with $x=0.4$, 0.5, 0.65, 0.8, 1.0, 1.2, and 1.5 was prepared. Figures 1 and 2 give, respectively, the x-ray-diffraction patterns and thermomagnetic scans of the $GdFe_{12-x}Nb_x$ alloys. From the experimental data, it can be seen that there are three different phase regions:

(i) For $x\leq 0.5$, the Th_2Zn_{17} structure ($T_c\cong 520$ K) is the main phase and the $ThMn_{12}$ structure is the second main phase ($T_c=597$ K), with some α-Fe impurity;

(ii) For $x\cong 0.65$, the $ThMn_{12}$ structure becomes a pure phase;

(iii) For $x\geq 0.8$, by increasing the Nb content the Th_2Zn_{17}-structure phase becomes dominant again with a significant amount of the $NbFe_2$ ($T_c=200$ K) phase.

Since both the $ThMn_{12}$ and Th_2Zn_{17} structures are related to $CaCu_5$,[17] the main phase changes from one to the other with the variation of Nb content. The homogeneous region of the $ThMn_{12}$-structure phase for $GdFe_{12-x}Nb_x$, around $x=0.65$, is narrower than those observed for other M elements in $YFe_{12-x}M_x$, e.g., $0.7\leq x\leq 1.25$ for Ti,[17] $1.25\leq x\leq 4.0$ for V,[18,19] $1.5\leq x\leq 3.5$ for Cr,[18] and $0.5\leq x\leq 4.0$ for Mo.[15] However, a quite low concentration of Nb is required to stabilize the $ThMn_{12}$-structure phase.

In the following, we shall show the experimental data of the series of $RFe_{11.35}Nb_{0,65}$ compounds, for $R=$Y, Sm, Gd, Tb, Dy, Ho, Er, and Lu, and the nitride analysis and discuss the results.

B. Crystallographic properties

The x-ray-diffraction analysis showed that all of the $RFe_{11.35}Nb_{0.65}$ alloys are single phase with the $ThMn_{12}$ structure, except for the Y compound which contains a little Y_2Fe_{17}. The nitrides retain the same structure, but some of them have a little α-Fe impurity. The nitrogen content y is about 1 in $RFe_{11.35}Nb_{0.65}N_y$, which was estimated by the weight difference for the sample before and after nitrogenation. Figure 3 gives the typical x-ray patterns for $LuFe_{11.35}Nb_{0.65}$ and its nitride. The variation of lattice constants a and c as a function of rare-earth element for $RFe_{11.35}Nb_{0.65}$ and $RFe_{11.35}Nb_{0.65}N_y$ are illustrated in Fig. 4 and their values are listed in Table I, together with $(\Delta V/V)\%$. The lattice parameters a and c for both of the parent alloys and their nitrides decrease with increasing atomic number of rare-earth elements R, due to the lanthanide contraction. The relative volume expansion is about 3% by nitrogena-

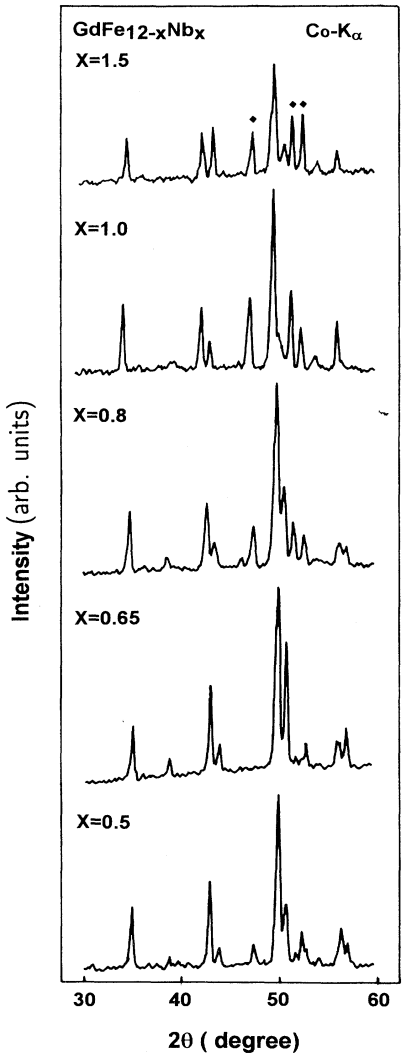

FIG. 1. X-ray-diffraction patterns of $GdFe_{12-x}Nb_x$ alloys (Co $K\alpha$ radiation) (the diamond symbols mark the reflections of Nb_2).

tion, which is similar to the other 1:12 nitrides.[4,5,7–11,15]

The $ErFe_{11.35}Nb_{0.65}$ compound was chosen for the neutron-powder-diffraction experiment for the study of Nb occupation in $ThMn_{12}$ structure. The powder-diffraction pattern of $ErFe_{11.35}Nb_{0.65}$ at room temperature is shown in Fig. 5. The data were analyzed with the Rietveld structure refinement program RIETAN.[20] Initially, the zero point, the background, and the parameters of the full width at half maximum, the lattice constants, and the profile parameters were refined. Secondly, the occupancies of Nb and Fe atoms at $8i$, $8j$, and $8f$ sites and the magnetic moments of Fe and R atoms were refined. We tried seven possibilities and found that the occupancy of Nb atoms exclusively on $8i$ sites is the best fit which has the lowest R_{WP} value of 8.4%. Here the weighted pattern factor

$$R_{WP}=\sum_i w_i[y_i(o)-y_i(c)]^2/\sum_i w_i y_i(o)^2 ,$$

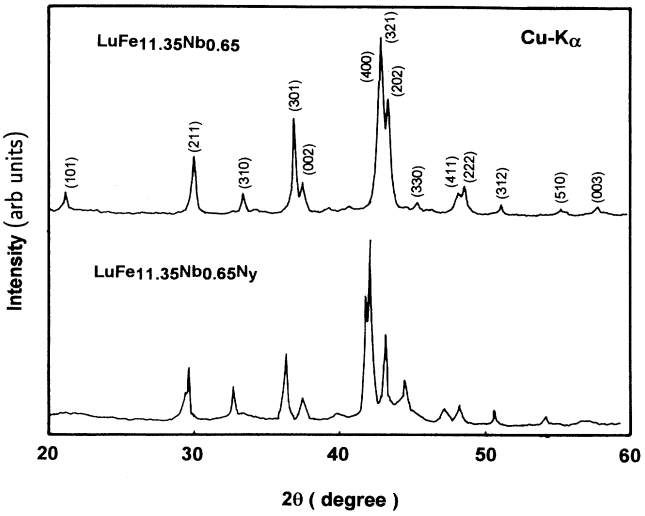

FIG. 3. X-ray-diffraction patterns of $LuFe_{11.35}Nb_{0.65}$ and $LuFe_{11.35}Nb_{0.65}N_y$ (Cu $K\alpha$ radiation).

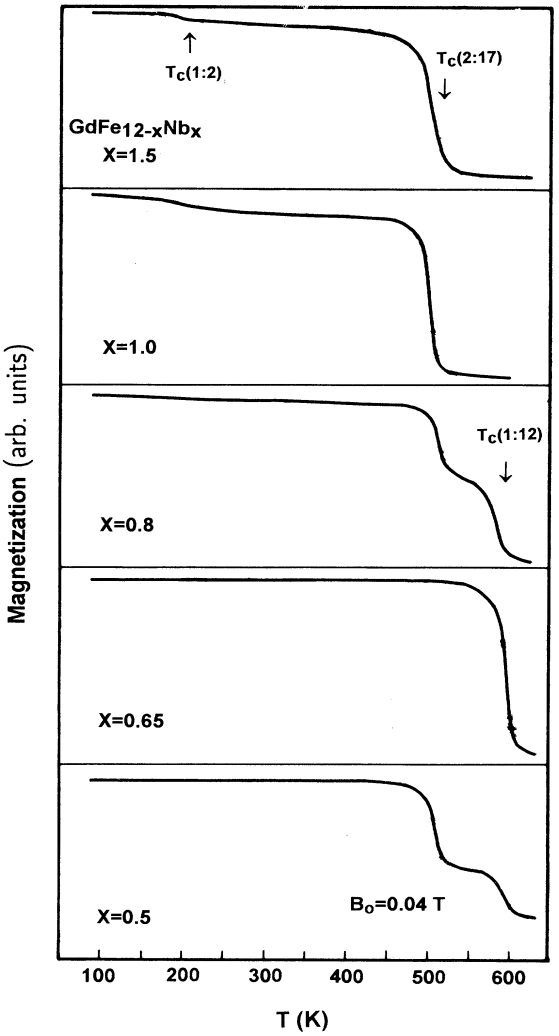

FIG. 2. Thermomagnetic curves of $GdFe_{12-x}Nb_x$ alloys in a magnetic field of 0.04 T. The three phases are marked by the arrows (see text).

where w_i, $y_i(o)$, and $y_i(c)$ are the weighted factor, the observed, and the calculated values at the ith point of the pattern, respectively; the summation was done for all points of the pattern. The final refined parameters are listed in Table II. The lattice constants are $a=0.847\,15(7)$ nm and $c=0.478\,31(5)$ nm, which are slightly lower than those observed from the x-ray-

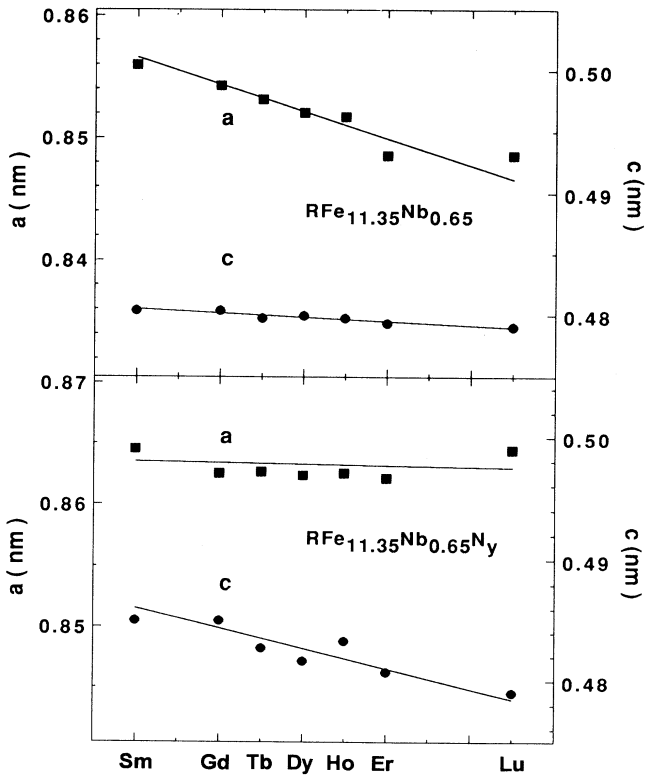

FIG. 4. Lattice constants a and c of $RFe_{11.35}Nb_{0.65}$ and $RFe_{11.35}Nb_{0.65}N_y$.

TABLE I. Structural and magnetic properties of $R\mathrm{Fe}_{11.35}\mathrm{Nb}_{0.65}$ and $R\mathrm{Fe}_{11.35}\mathrm{Nb}_{0.65}\mathrm{Ny}$.

Compound	a (nm)	c (nm)	$\Delta V/V$ (%)	T_c (K)	M_s (μ_B/f.u.) 1.5 K	M_s (μ_B/f.u.) 293 K	B_a (T) 1.5 K	B_a (T) 293 K
$\mathrm{YFe}_{11.35}\mathrm{Nb}_{0.65}$	0.8511	0.4790		526	21.3	18.0	3.60	2.06
$\mathrm{YFe}_{11.35}\mathrm{Nb}_{0.65}\mathrm{N}_y$	0.8634	0.4822	3.6	729	23.7	21.2	2.76	1.31
$\mathrm{SmFe}_{11.35}\mathrm{Nb}_{0.65}$	0.8560	0.4804		584	17.3	17.0	26.0	10.0
$\mathrm{SmFe}_{11.35}\mathrm{Nb}_{0.65}\mathrm{N}_y$	0.8646	0.4851	3.0	753	22.9	21.5		
$\mathrm{GdFe}_{11.35}\mathrm{Nb}_{0.65}$	0.8543	0.4804		597	15.0	14.2		3.55
$\mathrm{GdFe}_{11.35}\mathrm{Nb}_{0.65}\mathrm{N}_y$	0.8626	0.4851	3.0	773	17.7	16.9		1.53
$\mathrm{TbFe}_{11.35}\mathrm{Nb}_{0.65}$	0.8532	0.4798		556	12.0	13.1		
$\mathrm{TbFe}_{11.35}\mathrm{Nb}_{0.65}\mathrm{N}_y$	0.8627	0.4828	2.9	747	13.1	13.4		14.5
$\mathrm{DyFe}_{11.35}\mathrm{Nb}_{0.65}$	0.8521	0.4800		536	12.2	13.3		<1
$\mathrm{DyFe}_{11.35}\mathrm{Nb}_{0.65}\mathrm{N}_y$	0.8624	0.4817	2.8	737	12.7	13.1		11.5
$\mathrm{HoFe}_{11.35}\mathrm{Nb}_{0.65}$	0.8518	0.4798		520	11.0	12.8		2.45
$\mathrm{HoFe}_{11.35}\mathrm{Nb}_{0.65}\mathrm{N}_y$	0.8626	0.4834	3.3	723	12.7	15.4		
$\mathrm{ErFe}_{11.35}\mathrm{Nb}_{0.65}$	0.8486	0.4794		507	11.7	15.2		2.67
$\mathrm{ErFe}_{11.35}\mathrm{Nb}_{0.65}\mathrm{N}_y$	0.8622	0.4808	3.3	715	15.7	18.6		
$\mathrm{LuFe}_{11.35}\mathrm{Nb}_{0.65}$	0.8486	0.4791		489	20.6	16.9		
$\mathrm{LuFe}_{11.35}\mathrm{Nb}_{0.65}\mathrm{N}_y$	0.8645	0.4791	3.7	705	24.4	21.8		

diffraction analysis (see Table I).

We have found that the $M=\mathrm{Nb}$ in $R(\mathrm{Fe},M)_{12}$ only occupies the $8i$ sites, is similar to $M=\mathrm{Ti}$,[21] V,[22] or Mo,[23,24] and is different from $M=\mathrm{Si}$,[25] which occupies the $8f$ and $8j$ sites.

C. 3*d* magnetism (R=Y,Lu)

For the rare-earth–transition-metal (R-M) intermetallic compounds the M sublattice is so important that it determines the main magnetic properties of the compound, i.e., magnetization and Curie temperature. In order to understand the magnetic behavior of the $R\mathrm{Fe}_{11.35}\mathrm{Nb}_{0.65}$ and $R\mathrm{Fe}_{11.35}\mathrm{Nb}_{0.65}\mathrm{N}_y$ systems, we will show the data with non-magnetic $R=\mathrm{Y}$ and Lu and will discuss the effects of the 3*d*-electron magnetism of the Fe sublattice in $R\mathrm{Fe}_{11.35}\mathrm{Nb}_{0.65}$ and $R\mathrm{Fe}_{11.35}\mathrm{Nb}_{0.65}\mathrm{N}_y$.

1. Magnetization

Figure 6 shows the spontaneous magnetization of $\mathrm{YFe}_{11.35}\mathrm{Nb}_{0.65}$ and $\mathrm{YFe}_{11.35}\mathrm{Nb}_{0.65}\mathrm{N}_y$ as a function of temperature. At 1.5 K, the spontaneous magnetization is 21.2 μ_B/f.u. for $\mathrm{YFe}_{11.35}\mathrm{Nb}_{0.65}$, which is larger than those of the other 1:12 yttrium compounds, such as $\mathrm{YFe}_{11}\mathrm{Ti}$,[26] $\mathrm{YFe}_{10.4}\mathrm{V}_{1.6}$, $\mathrm{YFe}_{10}\mathrm{Cr}_2$, and $\mathrm{YFe}_{10.8}\mathrm{W}_{1.2}$,[27] but smaller than that of $\mathrm{YFe}_{11.5}\mathrm{Mo}_{0.5}$.[15] Some low-temperature (<4.2 K) saturation magnetization data of $\mathrm{YFe}_{12-x}M_x$ with some M elements are shown in Fig. 7. It can be seen that the magnetization of the Fe sublattice in $R\mathrm{Fe}_{12-x}M_x$ compounds increases almost linearly with decrease of the M content. Considering the average Fe atomic magnetic moment in $\mathrm{YFe}_{12-x}M_x$, we have $\mu_{\mathrm{Fe}}=1.73\mu_B$ for $M=\mathrm{Ti}$ ($x=1.0$),[26] $1.72\mu_B$ for V ($x=1.6$),[27] $1.67\mu_B$ for Cr ($x=2.0$),[27] $1.88\mu_B$ for Nb

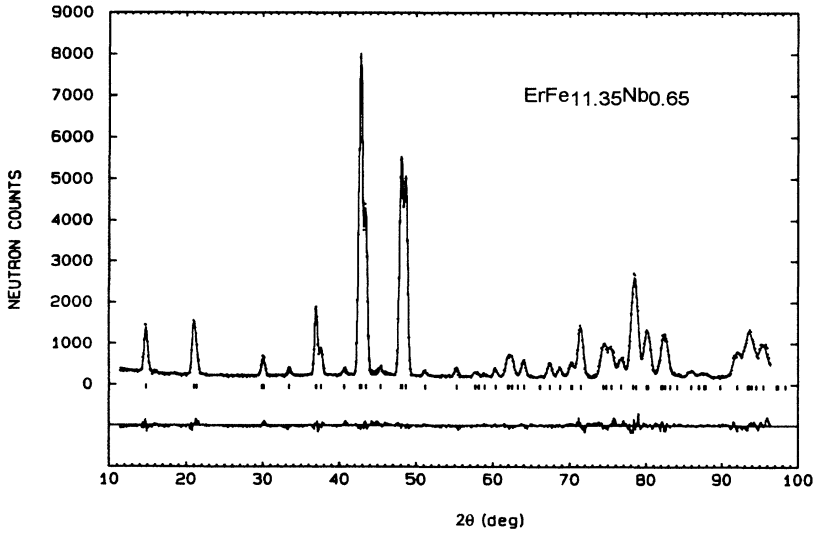

FIG. 5. Neutron-powder-diffraction patterns at a room temperature of 293 K for $\mathrm{ErFe}_{11.35}\mathrm{Nb}_{0.65}$: · · · ·, observed profiles; — — —, calculated curves; calculated positions are indicated at the bottom. The differences between the observed data and calculated values are also given.

TABLE II. Crystallographic and magnetic parameters of $ErFe_{11.35}Nb_{0.65}$ [tetragonal cell: space group $I4/mmm$; $a=0.847\,15(7)$ nm and $c=0.478\,31(5)$ nm].

Atom (site)	Occupancy	x	y	z	B (Å^2)	M (μ_B)
Er (2a)	1.0	0	0	0	0.67(10)	−3.4(5)
Nb (8i)	0.16	0.3565(5)	0	0	0.49(10)	0
Fe (8f)	1.0	0.2500	0.2500	0.2500	0.04	1.8(3)
Fe (8i)	0.84	0.3565(5)	0	0	0.49(10)	2.0(5)
Fe (8j)	1.0	0.2802(5)	0.5000	0	0.32(10)	1.9(5)

($x=0.65$), 2.14μ_B for Mo ($x=0.5$),[15] and 1.93μ_B for W ($x=1.2$).[27] These values indicate that the 4d or 5d elements have less effect in reducing the Fe magnetic moment than 3d elements in 1:12 compounds.

The neutron-diffraction analysis of $ErFe_{11.35}Nb_{0.65}$ at room temperature (see Table II) shows that Fe at the 8i site has the largest magnetic moment and Fe at the 8f site has the smallest magnetic moment, which is in accordance with the case found for the other 1:12 compounds.[1] The $LuFe_{11.35}Nb_{0.65}$ alloy has a little lower saturation magnetization than $YFe_{11.35}Nb_{0.65}$ (see Table I).

The spontaneous magnetization of the nitrides $RFe_{11.35}Nb_{0.65}N_y$ (R=Y,Lu) is enhanced by the interstitial N atoms (see Fig. 6 and Table I). The values of relative increase are 11.3% for Y and 18.4% for Lu. Taking the Fe atomic magnetic moment μ_{Fe} from Gd to Lu (see Table I), one may obtain the average value of the relative increase of the Fe-sublattice magnetization by nitrogenation of 11.2%. This Fe-sublattice magnetization enhancement by nitrogenation has also been observed in the other 1:12 nitrides[4,5,9,15] and 2:17 nitrides.[28,29] This increase of spontaneous magnetization may be related to the 3d band which is narrowed by the reduction of the R-Fe overlap[30,31] or by the volume expansion.[32]

For the magnetic moments of 3d transition-metal alloys, some pointers are provided by the magnetic valence model.[33,34] It ignores the details of the crystallographic environment and assumes strong ferromagnetism. In practice, an alloy can be considered to be a strong ferromagnet if the experimental magnetic-moment value lies on or between the two theoretical lines (where $\langle\mu\rangle$ and $\langle Z_m\rangle$ denote the average magnetic moment and the average magnetic valence, respectively) $\langle\mu\rangle=\langle Z_m\rangle+0.6$ and $\langle\mu\rangle=\langle Z_m\rangle+0.9$, while it is a weak ferromagnet if the experimental magnetic-moment value lies below the line $\langle\mu\rangle=\langle Z_m\rangle+0.6$. To date, this method has been quite successful, in the case of strong ferromagnets, when applied to explain a large amount of experimental data on the concentration dependence of binary transition-metal alloys,[33] transition-metal–metalloid alloys,[34] and rare-earth–transition-metal (Fe or Co) intermetallics.[1,35–37]

Figure 8 shows the average atomic magnetic moment $\langle\mu\rangle$ variation with average magnetic valence $\langle Z_m\rangle$ for some $ThMn_{12}$-structure yttrium compounds, compared with Fe, Co, and Ni. The points for many of the $ThMn_{12}$-structure alloys are close to the predicted lines corresponding to ferromagnets. The points for $YFe_{11.35}Nb_{0.65}$ and $YFe_{11}Ti$, lying below the line, are exceptional ones among the 1:12 compounds, which indicates that they are weak ferromagnets like Fe. However, by introducing N or C into the interstitial sites, although the magnetization of the Fe sublattice is enhanced, the average atomic magnetic moment $\langle\mu\rangle$ of yttrium 1:12

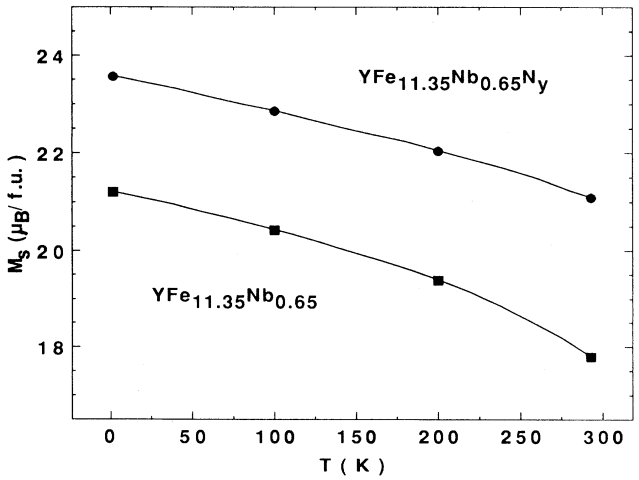

FIG. 6. Spontaneous magnetization as a function of temperature for $YFe_{11.35}Nb_{0.65}$ and $YFe_{11.35}Nb_{0.65}N_y$.

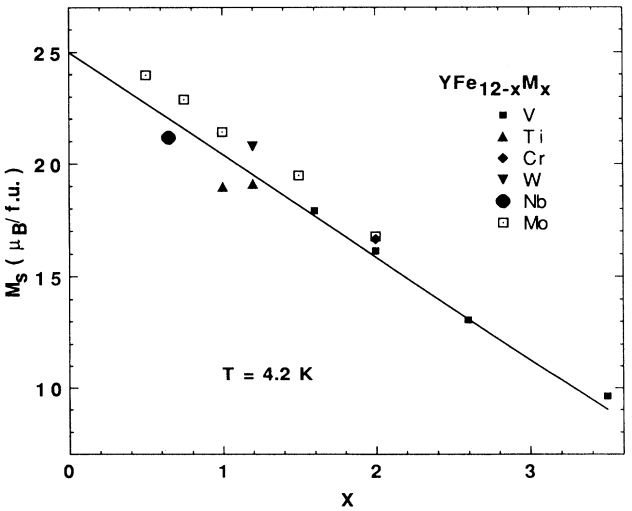

FIG. 7. Saturation magnetization at temperatures lower than 4.2 K as a function of M=Ti, V, Cr, Nb, Mo, and W in $YFe_{12-x}M_x$ alloys.

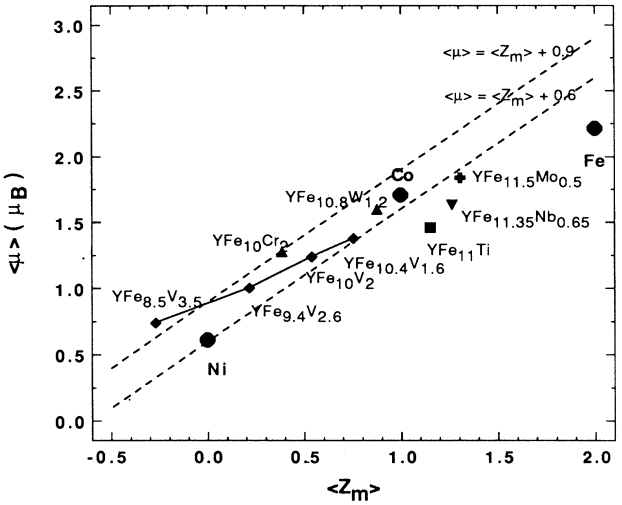

FIG. 8. Average atoms magnetic moment $\langle\mu\rangle$ as a function of average magnetic valence $\langle Z_m\rangle$ for $YFe_{12-x}M_x$ and $YFe_{12-x}M_xN_y$, including Fe, Co, and Ni for comparison.

(2:17) nitrides or carbides is still lower than the line $\langle\mu\rangle=\langle Z_m\rangle+0.6$ except for $YFe_{10}V_2N_y$ and $YFe_{11.5}Mo_{0.5}N_y$. The interstitial nitrogen and carbon are not taken into account in the model, because the assumption of a common band structure with a small Z occupancy for these elements is not valid. Band-structure calculations show isolated N or C levels 7–9 eV below the Fermi level.[30–32]

2. Curie temperature and exchange interaction

The exchange interactions in the rare-earth–iron intermetallics can be deduced in the molecular-field approximation from the expression for the magnetic ordering temperature[38]

$$T_c=\tfrac{1}{2}\{T_{\mathrm{Fe}}+[(T_{\mathrm{Fe}}-T_R)^2+4T_{R\mathrm{Fe}}^2]^{1/2}\}\ , \tag{3.1}$$

where T_{Fe}, T_R, and $T_{R\mathrm{Fe}}$ represent the contributions due to Fe-Fe, Fe-R, and R-R exchange interactions, respectively, and are given by

$$\begin{aligned} T_{\mathrm{Fe}}&=n_{\mathrm{FeFe}}C_{\mathrm{Fe}}\ ,\\ T_{RR}&=n_{RR}\gamma^2C_R\ ,\\ T_{R\mathrm{Fe}}&=n_{R\mathrm{Fe}}|\gamma|(C_{\mathrm{Fe}}C_R)^{1/2}\ , \end{aligned} \tag{3.2}$$

where

$$\begin{aligned} C_{\mathrm{Fe}}&=4N_{\mathrm{Fe}}S^*(S^*+1)\mu_B^2/3k_B\ ,\\ C_R&=N_Rg_J^2J(J+1)\mu_B^2/3k_B\ . \end{aligned} \tag{3.3}$$

Here, N_R and N_{Fe} are the number of R and Fe atoms per unit volume, $\gamma=2(g_J-1)/g$, and n_{FeFe}, n_{RR}, and $n_{R\mathrm{Fe}}$ are exchange-field coefficients. For a given series of Fe-R compounds, the n_{FeFe} (T_{Fe}) and n_{RR} (T_R) can be determined by means of isostructural nonmagnetic rare-earth compounds (Y-M, La-M, or Lu-M) and nonmagnetic or poorly magnetic transition-metal compounds (R-Cu, R-Mn, R-Ni, and so on), respectively. Since R-R interactions are very weak, n_{RR} may usually be neglected without significant effect. For $ThMn_{12}$-structure compounds, an n_{RR} value of 30 μ_0–350μ_0 has been deduced from the ordering temperature in the RCu_4Al_8 series,[37] which has only a 2% effect on the value of $n_{R\mathrm{Fe}}$, because of the small R concentration in the structure.

The Fe-Fe exchange interactions of the $RFe_{11.35}Nb_{0.65}$ and $RFe_{11.35}Nb_{0.65}N_y$ systems can be deduced from the Curie temperatures of the compounds with R=Y and Lu, especially the Lu compound which has the same $5d/6s$ structure as the rest of the series, and a nonmagnetic $4f^{14}$ shell. $2[S^*(S^*+1)]^{1/2}\mu_B$ is the Fe atomic effective moment in the paramagnetic state, taken as $3.70\mu_B$ from a comparison of the paramagnetic susceptibility of related compounds (RFe_2, RFe_3, R_2Fe_{17}, $R_2Fe_{14}B$).[38–40] Taking the average volume values of 0.1742 nm^3 of the whole $RFe_{11.35}Nb_{0.65}$ series and 0.1798 nm^3 of the whole $RFe_{11.35}Nb_{0.65}$ N_y series, we obtain $n_{\mathrm{FeFe}}=226\mu_0$ (T_c=526 K) from $YFe_{11.35}Nb_{0.65}$ or $n_{\mathrm{FeFe}}=210\mu_0$ (T_c=489 K) from $LuFe_{11.35}Nb_{0.65}$, and $n_{\mathrm{FeFe}}=323\mu_0$ (T_c=729 K) from $YFe_{11.35}Nb_{0.65}N_y$ or $n_{\mathrm{FeFe}}=312\mu_0$($T_c$=705 K) from $LuFe_{11.35}Nb_{0.65}N_y$, respectively. By the effect of interstitial N atoms, the exchange interaction of the Fe sublattice in $RFe_{11.35}Nb_{0.65}$ (R=Y and Lu) is enhanced about 45%, which is similar to the value found in the $YFe_{12-x}Mo_x$ series.[15]

3. Magnetocrystalline anisotropy of the Fe sublattice

The Fe sublattices of the $RFe_{11.35}Nb_{0.65}$ and $RFe_{11.35}Nb_{0.65}N_y$ series,[41] as well as of the other $RFe_{12-x}M_x$ alloys[1] with their nitrides,[4,9,42,43] have easy c-axis anisotropy. The value of the anisotropy constant K_1(Fe) for $YFe_{11.35}Nb_{0.65}$ and $YFe_{11.35}Nb_{0.65}N_y$ has been obtained from the B_a(Fe) data measured by the SPD technique,[16] with the relation $K_1(\mathrm{Fe})=\frac{1}{2}B_a(\mathrm{Fe})M_s(\mathrm{Fe})$, where M_s(Fe) is the saturation magnetization of the Fe sublattice. Figure 9 shows the anisotropy constant K_1(Fe) as a function of temperature for $YFe_{11.35}Nb_{0.65}$ and $YFe_{11.35}Nb_{0.65}N_y$, respectively. It can be seen that the K_1(Fe) is weakened by the interstitial N atoms. This has been found also in the other 1:12 systems[9,42,43] and 2:17 systems.[44] At a temperature of 1.5 K, the values of K_1(Fe) are 25.7 and 21.9 K/f.u. for $YFe_{11.35}Nb_{0.65}$ and $YFe_{11.35}Nb_{0.65}N_y$, respectively, and at 293 K values of K_1(Fe) are 12.7 and 10.1 K/f.u. The decrease of K_1(Fe) by nitrogenation at 1.5 K is about 17%.

For 1:12 compounds, the major contribution to the uniaxial anisotropy of the Fe sublattice comes from the 8i sites.[17] It would be expected that $YFe_{12-x}M_x$ may have stronger Fe-sublattice anisotropy with lower M concentration at 8i sites. But the situation is not simple, because different M elements have different effects on the Fe sublattice although they occupy the same crystallographic sites. For example, Ti, V, Mo, and Nb occupy 8i sites, but $YFe_{12-x}Mo_x$ has much smaller K_1(Fe) than $YFe_{12-x}M_x$ (M=Ti, V, or Nb), even if the former has a lower x value than the latter.[27,29,42,43] However, the

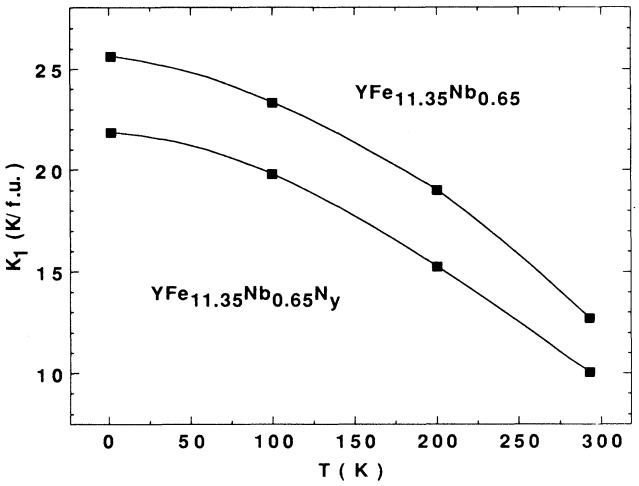

FIG. 9. Temperature dependence of the anisotropy constant K_1(Fe) in $YFe_{11.35}Nb_{0.65}$ and $YFe_{11.35}Nb_{0.65}N_y$, respectively.

K_1(Fe) of $YFe_{12-x}Mo_x$ decreases with increasing Mo concentration x.[42,43] Among all the 1:12 alloys discovered so far, $YFe_{11.35}Nb_{0.65}$ has the largest K_1(Fe).

D. 4*f* magnetism

In the rare-earth–transition-metal (R-M) intermetallic compounds, a large variety of interesting magnetic properties is strongly dependent on R, which underlines the important role of the magnetic $4f$-electron shell in the system. In this section, we will show the experimental data of the magnetic properties of $RFe_{11.35}Nb_{0.65}$ and $RFe_{11.35}Nb_{0.65}N_y$ with magnetic R and then analyze and discuss the $4f$ magnetism in terms of exchange and crystal-field interactions.

1. R-Fe exchange interactions

Having discussed the Fe-Fe exchange interactions above, we now turn to investigate the exchange interactions between the Fe and R sublattices in the $RFe_{11.35}Nb_{0.65}$ and $RFe_{11.35}Nb_{0.65}N_y$ series, respectively.

The Curie temperature in the $RFe_{11.35}Nb_{0.65}$ or $RFe_{11.35}Nb_{0.65}N_y$ series varies with R as shown in Fig. 10 (values are also listed in Table I). There is a familiar maximum at Gd, similar to the other rare-earth–iron alloys and nitrides,[1,2,4–6,39] which is due to Gd^{3+} having the largest spin moment.

The R-Fe exchange interactions can be deduced from the molecular-field approximation using the expression for the magnetic ordering temperature.[38] Neglecting the R-R interactions, the exchange-field coefficient is given by (see Sec. III C 2)

$$n_{R\mathrm{Fe}}=[(T_c-T_{\mathrm{Fe}})T_c]^{1/2}/|\gamma|(C_{\mathrm{Fe}}C_R)^{1/2}\ . \tag{3.4}$$

Taking the Fe-sublattice ordering temperature $T_{\mathrm{Fe}}=489$ and 705 K from $LuFe_{11.35}Nb_{0.65}$ and $LuFe_{11.35}Nb_{0.65}N_y$, respectively, and the average volume of the $RFe_{11.35}Nb_{0.65}$ and $RFe_{11.35}Nb_{0.65}N_y$ series as 0.1742 and 0.1798 nm^3, respectively, we obtain the values of $n_{R\mathrm{Fe}}$ for

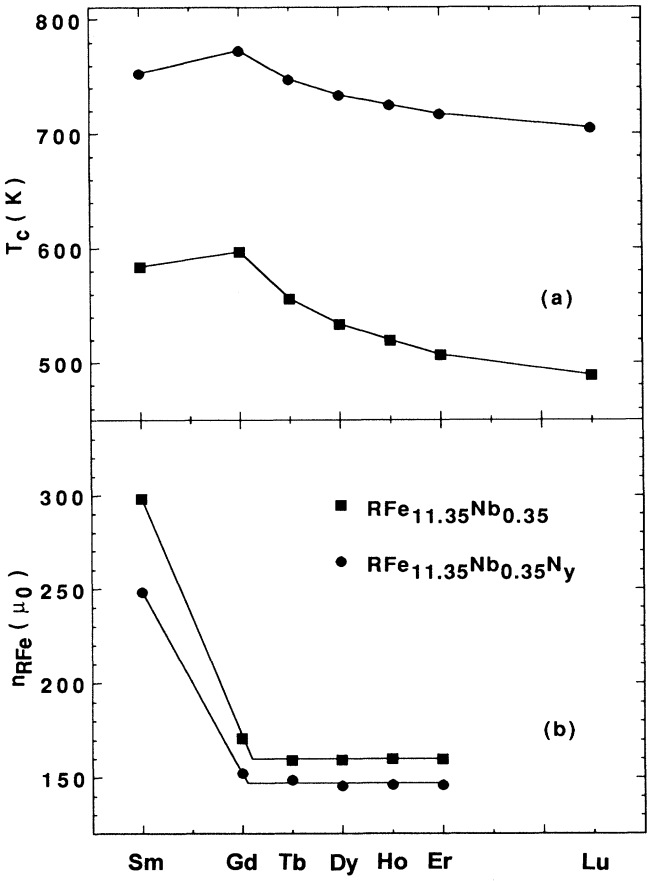

FIG. 10. Rare-earth-element dependence of Curie temperatures (a) and corresponding R-Fe exchange coefficients (b) for the $RFe_{11.35}Nb_{0.65}$ and $RFe_{11.35}Nb_{0.65}N_y$ series, respectively.

both series as plotted in Fig. 10. It can be seen that $n_{R\mathrm{Fe}}$ decreases across the lanthanide series. The $n_{R\mathrm{Fe}}$ value is roughly twice as large for light rare-earth-atoms as for heavy rare-earth-atoms in both series of parent compounds and nitrides, which is similar to many other R-Fe intermetallic compounds.[26,37,38,45] The systematic decrease of $n_{R\mathrm{Fe}}$ by a factor of 2 or more from the light rare-earth elements to the heavy rare-earth elements appears to be a general feature of rare-earth intermetallic compounds and it may be related to $4f$-$5d$ overlap.[38,46,47] It also can be seen the R-Fe exchange interactions are slightly weakened for the nitrides on average ($\langle n_{R\mathrm{Fe}}\rangle=147\mu_0$ for heavy rare-earth elements) compared with the parent compounds ($\langle n_{R\mathrm{Fe}}\rangle=160\mu_0$ for heavy rare-earth elements), which has also been found in the other nitrides or carbides.[6,45] This reduction by nitrogenation or carbonation may also be attributed to the lattice volume expansion or the formation of covalent bonds by valence electrons of rare-earth atoms with $2p$ electrons of N or C to reduce the $4f$-$5d$ overlap.[6] By the analysis of exchange interactions above, we may conclude that the enhancement of the Curie temperature by nitrogenation or carbonation is contributed by the strengthened Fe-Fe exchange interactions (see Sec. III C 2) rather than by R-Fe interactions.

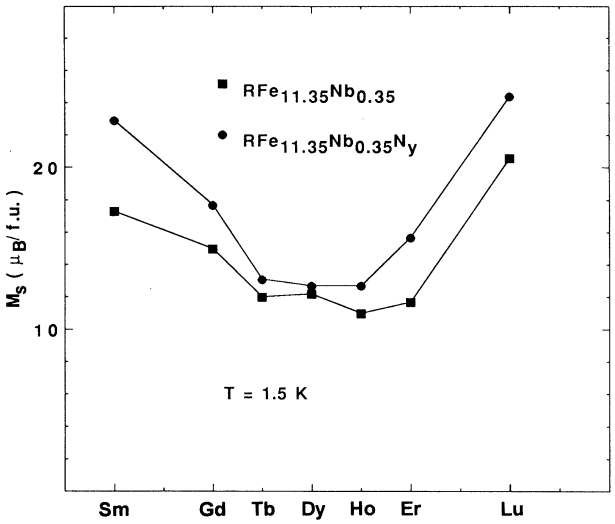

FIG. 11. Rare-earth-element dependence of saturation magnetization values at 1.5 K for the $R\mathrm{Fe}_{11.35}\mathrm{Nb}_{0.65}$ and $R\mathrm{Fe}_{11.35}\mathrm{Nb}_{0.65}\mathrm{N}_y$ series, respectively.

2. *Magnetic structure*

The saturation magnetization values of $R\mathrm{Fe}_{11.35}\mathrm{Nb}_{0.65}$ and $R\mathrm{Fe}_{11.35}\mathrm{Nb}_{0.65}\mathrm{N}_y$ compounds are summarized in Table I and illustrated in Fig. 11. The saturation magnetization with all the heavy rare-earth elements is considerably less than that of the Fe sublattice as measured for $R=$Y or Lu. This suggests the conventional coupling scheme of iron and rare-earth atom moments is antiparallel for the heavy-earth elements. The neutron-powder-diffraction experiment on $\mathrm{ErFe}_{11.35}\mathrm{Nb}_{0.65}$ at room temperature also shows that the magnetic moment of Er is antiparallel to those of Fe (Table II). Assuming the R atomic magnetic moment $\mu_R=g_J J\mu_B$, the Fe atomic magnetic moment μ_{Fe} can be deduced (Table I). Taking the average value, we obtain $\langle\mu_{\mathrm{Fe}}\rangle=1.87\mu_B$ for the parent alloys and $2.08\mu_B$ for their nitrides. These values are almost the same as those for the yttrium alloy and its nitride, respectively.

X-ray-diffraction patterns on the oriented samples showed that at room temperature the $R\mathrm{Fe}_{11.35}\mathrm{Nb}_{0.65}$ has easy c-axis anisotropy for all the rare-earth atoms except for Tb and $R\mathrm{Fe}_{11.35}\mathrm{Nb}_{0.65}\mathrm{N}_y$ has easy c-axis anisotropy for all the rare-earth atoms except for Sm and Er. The anisotropy difference between the parent compounds and the nitrides is due to the sign change of the second-order crystal-field coefficient A_{20}.[48] $\mathrm{SmFe}_{11.35}\mathrm{Nb}_{0.65}$ has the strongest anisotropy field among all the alloys, with $B_a=26.0$ T at 1.5 K and 10.0 T at 293 K. We did not observe the first-order magnetization process [FOMP Ref. (16)] at low temperature in $\mathrm{SmFe}_{11.35}\mathrm{Nb}_{0.65}$, unlike in $\mathrm{SmFe}_{11}\mathrm{Ti}$.[29] For the nitrides, $R\mathrm{Fe}_{11.35}\mathrm{Nb}_{0.65}\mathrm{N}_y$ ($R=$Dy or Tb) has a strong anisotropy field (Table I).

Curves of ac susceptibility measurements and magnetization variation as a function of temperature in an applied field of 0.045 T for the heavy rare-earth alloys and their nitrides are shown, respectively, in Figs. 12 and 13. The data for $R\mathrm{Fe}_{11.35}\mathrm{Nb}_{0.65}$ with $R=$Dy and Er show an anomalous temperature variation which will be associated with spin reorientation, but we did not observe spin-reorientation transitions in the other alloys and nitrides. It can be seen that there are two steps for $\mathrm{DyFe}_{11.35}\mathrm{Nb}_{0.65}$ at $T_{\mathrm{sr1}}=160$ K and $T_{\mathrm{sr2}}=245$ K, which is similar to the case observed for $\mathrm{DyFe}_{11}\mathrm{Ti}$.[26] For $\mathrm{ErFe}_{11.35}\mathrm{Nb}_{0.65}$, the magnetization cants from the c axis at $T_{\mathrm{sr}}=41$ K, which is similar to the case observed for $\mathrm{ErFe}_{11}\mathrm{Ti}$.[26] At room temperature and above, the uniaxial iron anisotropy usually determines the magnetization direction but at low temperatures the rare-earth anisotropy may be dominant. The exceptions are $\mathrm{TbFe}_{11.35}\mathrm{Nb}_{0.65}$, $\mathrm{SmFe}_{11.35}\mathrm{Nb}_{0.65}\mathrm{N}_y$, and $\mathrm{ErFe}_{11.35}\mathrm{Nb}_{0.65}\mathrm{N}_y$, for which the magnetization vectors are not along the c axis at room temperature.

The magnetic structures as a function of temperature in the $R\mathrm{Fe}_{11.35}\mathrm{Nb}_{0.65}$ and $R\mathrm{Fe}_{11.35}\ \mathrm{Nb}_{0.65}\mathrm{N}_y$ series are shown in Fig. 14.

3. *Crystal-field interactions in* $R\mathrm{Fe}_{11.35}\mathrm{Nb}_{0.65}$

The exchange- and crystal-field-interaction model, described in Refs. 49 and 50, is used here to explain the complex magnetic behavior in the $R\mathrm{Fe}_{11.35}\mathrm{Nb}_{0.65}$ series.

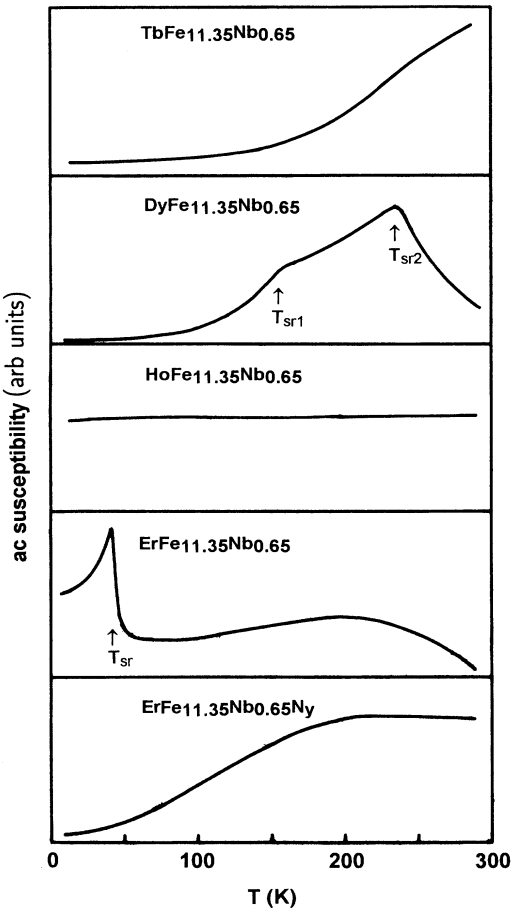

FIG. 12. Temperature dependence of the ac susceptibility of $R\mathrm{Fe}_{11.35}\mathrm{Nb}_{0.65}$ ($R=$Tb,Dy,Ho,Er) and $\mathrm{ErFe}_{11.35}\mathrm{Nb}_{0.65}\mathrm{N}_y$ (the spin-reorientation transitions are marked by the arrows).

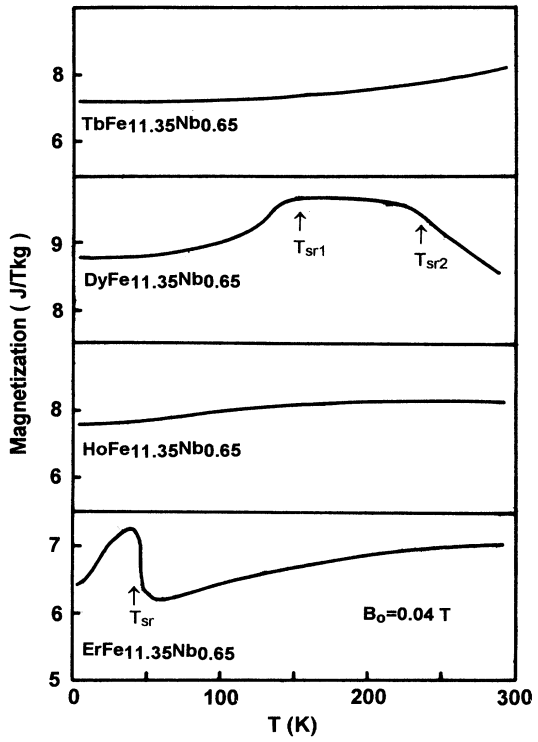

FIG. 13. Thermomagnetic curves of $R\mathrm{Fe}_{11.35}\mathrm{Nb}_{0.65}$ (the spin-reorientation transitions are marked by the arrows.)

The crystal-field Hamiltonian at the rare-earth $2a$ sites in the ThMn_{12} structure (point symmetry $4/mmm$) is

$$H_{\mathrm{CF}}=B_{20}O_{20}+B_{40}O_{40}+B_4O_{44}+B_{60}O_{60}+B_{64}O_{64}\ , \tag{3.5}$$

where $\{B_{nm}\}$ ($B_{nm}=\theta_n A_{nm}\langle r^n\rangle$ for rare-earth ions except the J-mixing Sm^{3+}) are crystal-field parameters depending on the specific rare-earth ion and $\{O_{nm}(J)\}$ are the Stevens equivalent operators.[51]

In our analysis, the temperature dependence of the Fe-sublattice magnetization $\mathbf{M}_{\mathrm{Fe}}$ and the anisotropy constant K_1(Fe) were taken from $\mathrm{YFe}_{11.35}\mathrm{Nb}_{0.65}$ (see Secs. III C 1 and III C 3). The five crystal-field coefficients $\{A_{nm}\}$ were taken to be those obtained from fitting the single-crystal magnetization curves for $\mathrm{DyFe}_{11}\mathrm{Ti}$:[50] $A_{20}=-32.3$ Ka_0^{-2}, $A_{40}=-12.4$ Ka_0^{-4}, $A_{44}=118$ Ka_0^{-4}, $A_{60}=-2.56$ Ka_0^{-6}, and $A_{64}=0.64$ Ka_0^{-6} (where a_0 is the Bohr radius). The exchange coefficient $n_{R\mathrm{Fe}}=160\mu_0$ for all the heavy rare-earth atoms deduced from the Curie temperatures (see Sec. III D 1). Therefore the magnetic-structure variation with temperature may be calculated.

Since the aspherical orbital wave functions of $4f$ electrons interact strongly with the crystal field, the rare-earth ions make a great contribution to the anisotropy for the R-M intermetallics. The anisotropy of a rare-earth ion with tetragonal symmetry, as in our $R\mathrm{Fe}_{11.35}\mathrm{Nb}_{0.65}$ system, may be described by the phenomenological expression

$$E_R^a=K_1(R)\sin^2\theta+[K_2(R)+K_2'(R)\cos4\phi]\sin^4\theta$$
$$+[K_3(R)+K_3'(R)\cos4\phi]\sin^6\theta\ , \tag{3.6}$$

where θ and ϕ are polar angles of the magnetization vector in the reference frame where **x** is parallel to [100] and **z** is parallel to [001]. The relationship between the anisotropy constants $\{K_i\}$ for the rare-earth and the crystal-field parameters $\{B_{nm}\}$ can be obtained by a rota-

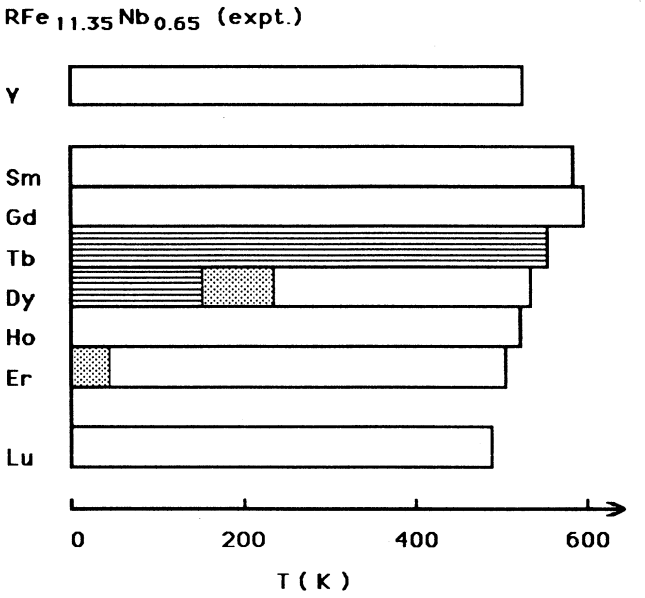

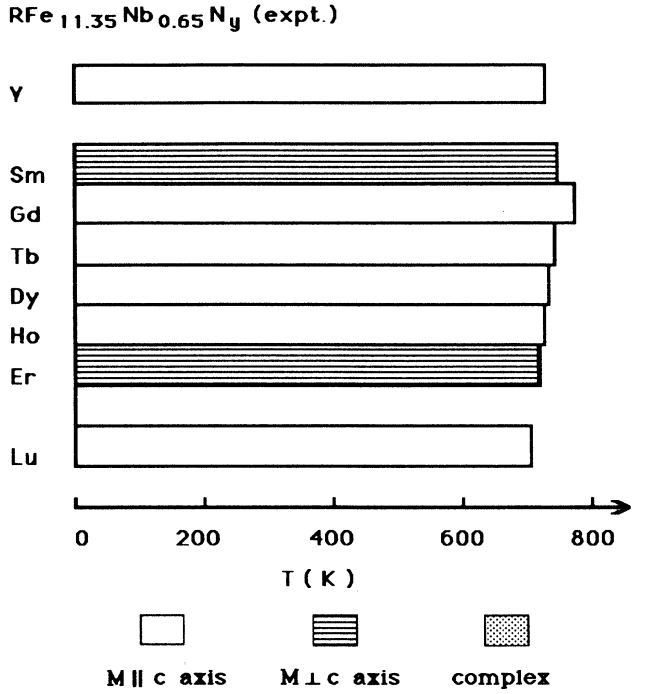

FIG. 14. Observed temperature variation of the magnetic structure of $R\mathrm{Fe}_{11.35}\mathrm{Nb}_{0.65}$ and $R\mathrm{Fe}_{11.35}\mathrm{Nb}_{0.65}\mathrm{N}_y$ series, respectively.

tion transformation of crystal-field terms[52]

$$
\begin{aligned}
K_1(R) &= -[\tfrac{3}{2}B_{20}\langle O_{20}\rangle + 5B_{40}\langle O_{40}\rangle + \tfrac{21}{2}B_{60}\langle O_{60}\rangle] ,\\
K_2(R) &= \tfrac{7}{8}[5B_{40}\langle O_{40}\rangle + 27B_{60}\langle O_{60}\rangle] ,\\
K_2'(R) &= \tfrac{1}{8}[B_{44}\langle O_{40}\rangle + 5B_{64}\langle O_{60}\rangle] ,\\
K_3(R) &= -\tfrac{231}{16}B_{60}\langle O_{60}\rangle ,\\
K_3'(R) &= -\tfrac{11}{16}B_{64}\langle O_{60}\rangle ,
\end{aligned}
\tag{3.7}
$$

where $\{\langle O_{nm}\rangle\}$ are thermal average values of the matrix elements of Stevens operator equivalents.

The magnetization direction in the compounds is determined by the crystal-field terms according to the anisotropy energy $E_{\rm tot}^a = K_1(\mathrm{Fe})\sin^2\theta_{\rm Fe} + E_R^a$, in which the factor of rare-earth-atom number per formula in front of E_R^a has been put as 1 for our 1:12 structure. In the plane containing the c axis the anisotropy depends on $K_1(\mathrm{Fe})$, $K_i(R)$ $(i=1,2,3)$, and $K_i(R)'$ $(i=2,3)$, while in the plane perpendicular to the c axis the anisotropy depends only on $K_i(R)'(i=2,3)$. The mixing effects of $K_1(\mathrm{Fe})$, $K_i(R)$, and $K_i(R)'$ give the tilting angle and $K_i(R)'$ determines the angular component in the plane. Generally, one finds

$$\theta=0^\circ \text{ if } K_1(\mathrm{Fe})+K_1(R)+K_2(R)+K_3(R)-|K_2'(R)+K_3'(R)|>0 \text{ and } K_1(\mathrm{Fe})+K_1(R)>0 , \tag{3.8}$$

$$
\begin{aligned}
&\theta=90^\circ \text{ and } \phi=0^\circ\\
&\quad \text{if } K_1(\mathrm{Fe})+K_1(R)+[K_2(R)+K_2'(R)]+[K_3(R)+K_3'(R)]<0 ,\\
&\qquad K_1(\mathrm{Fe})+K_1(R)+2[K_2(R)+K_2'(R)]+3[K_3(R)+K_3'(R)]<0, \text{ and } K_2'(R)+K_3'(R)<0 ,
\end{aligned}
\tag{3.9}
$$

$$
\begin{aligned}
&\theta=90^\circ \text{ and } \phi=45^\circ\\
&\quad \text{if } K_1(\mathrm{Fe})+K_1(R)+[K_2(R)-K_2'(R)]+[K_3(R)-K_3'(R)]<0 ,\\
&\qquad K_1(\mathrm{Fe})+K_1(R)+2[K_2(R)-K_2'(R)]+3[K_3(R)-K_3'(R)]<0, \text{ and } K_2'(R)+K_3'(R)>0 .
\end{aligned}
\tag{3.10}
$$

Otherwise it is given by

$$\sin^2\theta = \frac{(-[K_2(R)+K_2'(R)\cos4\phi]\pm\{[K_2(R)+K_2'(R)\cos4\phi]^2-3[K_1(\mathrm{Fe})+K_1(R)][K_3(R)+K_3'(R)\cos4\phi]\}^{1/2})}{3[K_3(R)+K_3'(R)\cos4\phi]} \tag{3.11}$$

with

$$\phi = \begin{cases} 0 & \text{if } K_2'(R)+K_3'(R)\sin^2\theta<0 ,\\ 45^\circ & \text{if } K_2'(R)+K_3'(R)\sin^2\theta>0 , \end{cases}$$

or

$$\sin^2\theta = \{-K_2(R)\pm[K_2(R)^2-3[K_1(\mathrm{Fe})+K_1(R)]K_3(R)]^{1/2}\}/3K_3(R) \tag{3.12}$$

when

$$K_2'(R)+K_3'(R)\sin^2\theta=0 .$$

Since the values of $B_{64}\langle O_{60}\rangle$ are much smaller than those of $B_{44}\langle O_{40}\rangle$ (about 5%), in our $R\mathrm{Fe}_{11.3}\mathrm{Nb}_{0.65}$ series, as in the $R\mathrm{Fe}_{11}\mathrm{Ti}$ series,[37] the planar anisotropy is actually dominated by the $B_{44}\langle O_{40}\rangle$ term. As $A_{44}>0$ $(B_{44}=\beta_J A_{44}\langle r^4\rangle)$, the easy magnetization direction in the (001) plane is along [100] for Dy and Ho $(\beta_J<0$, $K_2'(R)<0)$ and is along [110] for Tb and Er $(\beta_J>0$, $K_2'(R)>0)$, which is illustrated in Fig. 15 showing the calculated energy-surface variations with ϕ in the (001) plane at a temperature of 4.2 K.

The energy-surface variation in the (110) plane with temperature for $\mathrm{TbFe}_{11.35}\mathrm{Nb}_{0.65}$ is shown in Fig. 16. At $T=4.2$ K, the minimum at $\theta=90^\circ$ is lower than the one at $\theta=0^\circ$. With increasing temperature, the minimum at $\theta=0^\circ$ becomes lower when $T\geq 168$ K, and the easy magnetization direction of $\mathrm{TbFe}_{11.35}\mathrm{Nb}_{0.65}$ jumps from in the c plane to along the c axis, which is not in agreement with observations which show planar anisotropy at room temperature and no spin reorientation down to 1.5 K (see Figs. 12 and 13 and Sec. III D 2). The discrepancy here for the Tb compound, which was also found similarly in the $R\mathrm{Fe}_{11}\mathrm{Te}$ series,[50] might be attributed to the small admixture of the Tb^{4+} $(4f^7)$ state to double the effective $B_{20}O_{20}$ interaction.[37]

Figure 17 shows the calculated energy surfaces in the (010) plane of $\mathrm{DyFe}_{11.35}\mathrm{Nb}_{0.65}$ at some temperatures. At $T=4.2$ K, there are two nearly degenerate energy minima in the total energy surface, one at $\theta=43.5^\circ$ and the other $\theta=90^\circ$. When $T<85$ K, the energy is lowest for $\theta=90^\circ$, but as the temperature increases $(85\leq T\leq 230$ K) the energy minimum corresponding to an intermediate angle is lower. This angle decreases gradually with increasing temperature and finally becomes zero when $T>230$ K. The two calculated spin-reorientation transition temperatures are $T_{\rm sr1}^{\rm calc}=85$ K and $T_{\rm sr2}^{\rm calc}=230$ K, compared to the experimental values of $T_{\rm sr1}=160$ K and $T_{\rm sr2}=235$ K. Since the spin-reorientation transition temperatures were deduced from the temperature dependence of magnetization and ac susceptibility of the polycrystalline sample, the lower transition temperature value $(T_{\rm sr1})$ may be much bigger than the more precise value

which can be obtained on single crystal, as is the case for $DyFe_{11}Ti$.[50,53,54]

The calculated energy surfaces in Fig. 18 show that $HoFe_{11.35}Nb_{0.65}$ has easy c-axis anisotropy at all temperatures. There are two minima in the energy surface of $HoFe_{11.35}Nb_{0.65}$ at low temperature, but the one at $\theta=0°$ is always lower. When $T>100$ K; there is only one minimum at $\theta=0°$. Since the second-order Stevens coefficient α_J of Ho^{3+} is negative and then $B_{20}\langle O_{20}\rangle=6.4$ K and $B_{40}\langle O_{40}\rangle=12.4$ K, it is expected that $HoFe_{11.35}Nb_{0.65}$ may have a spin-reorientation transition at low temperature. However, $K_1(\mathrm{Fe})=25.7$ K/f.u., $K_1(R)=199.3$ K/f.u., and

$$K_{\mathrm{eff}}(R)=K_1(R)+K_2(R)+K_3(R)-|K_2'(R)+K_3'(R)|$$
$$=-10.1 \text{ K/f.u.}$$

at $T=0$ K, which meet the conditions in Eq. (3.8), so that the magnetization of $HoFe_{11.35}Nb_{0.65}$ always stays along the c axis. Since the two minima at $\theta=0°$ and $\theta=55°$ are almost degenerate at low temperature, weakening of the transition-metal anisotropy is expected to lead to an intermediate spin reorientation. Spin-reorientation transitions have been observed in

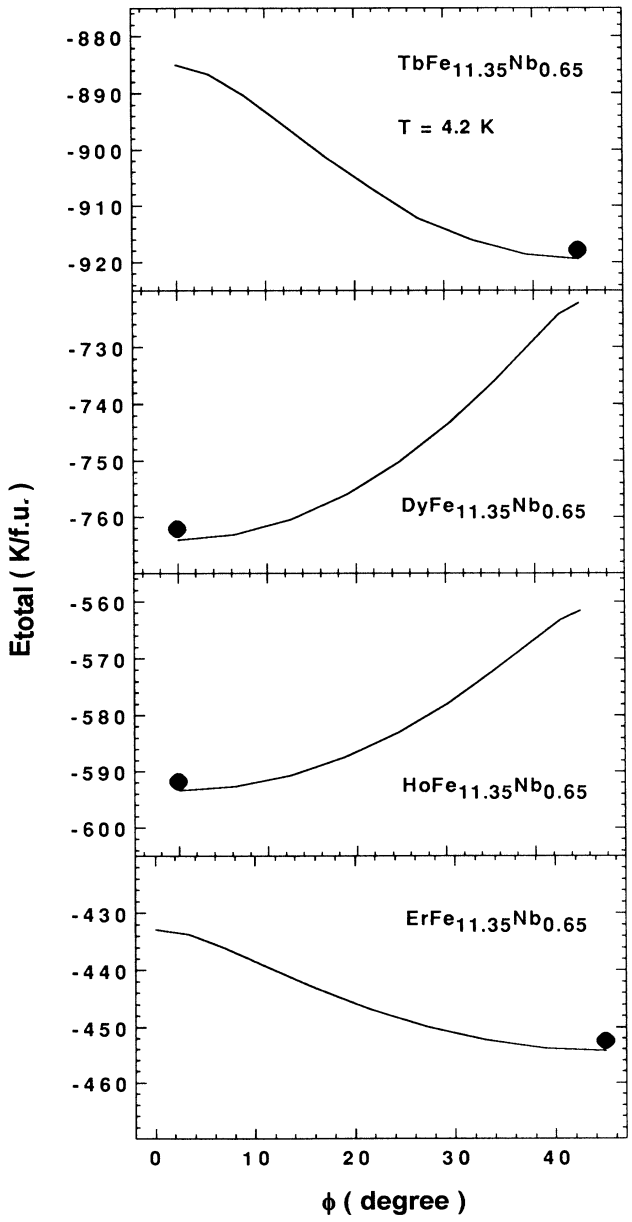

FIG. 15. Calculated energy surfaces in the (001) plane at 4.2 K for $RFe_{11.35}Nb_{0.65}$.

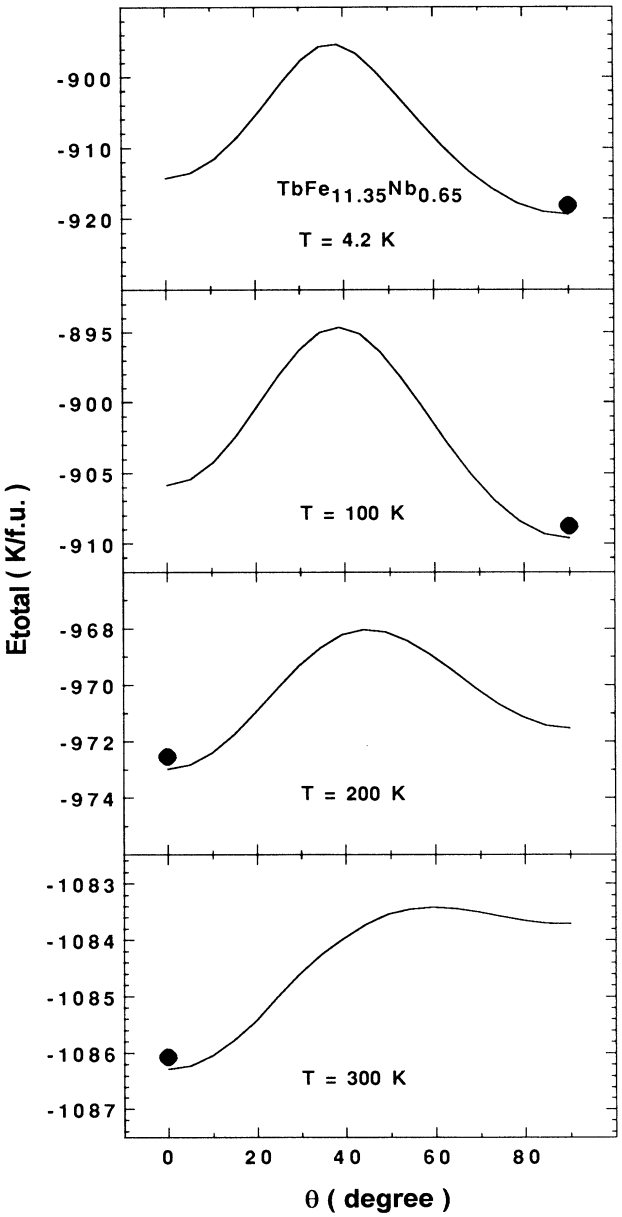

FIG. 16. Calculated energy surfaces in the (110) plane of $TbFe_{11.35}Nb_{0.65}$. The energy minima are $\theta=90°$ at 4.2 K, $\theta=90°$ at 100 K, $\theta=0°$ at 200 K, and $\theta=0°$ at 300 K, shown by black circles.

$HoFe_{10}M_2$ (M=V and Mo) compounds at low temperature.[55]

Unlike $HoFe_{11.35}Nb_{0.65}$, $ErFe_{11.35}Nb_{0.65}$, with a positive α_J of Er^{3+}, has a spin reorientation at low temperature (see Figs. 12 and 13). The calculated energy surface shows that the minimum at T=4.2 K is at θ=22.5° (see Fig. 19). In this compound, the iron and the rare-earth-atom second-order anisotropy both favor the c axis, while $B_{20}\langle O_2\rangle=-6.12$ K, $B_{40}\langle O_{40}\rangle=-11.4$ K, $B_{44}\langle O_{40}\rangle=109$ K, $B_{60}\langle O_{60}\rangle=23.0$ K, and $B_{64}\langle O_{60}\rangle=5.7$ K at 0 K. The conditions in Eq. (3.8) for θ=0° are not held, with

$$K_1(\mathrm{Fe})+K_1(R)+K_2(R)+K_3(R)-|K_2'(R)+K_3'(R)| = -12.26\ \mathrm{K} < 0 ,$$

and

$$K_1(\mathrm{Fe})+K_1(R) = -149.6\ \mathrm{K} < 0 ,$$

so that the magnetization is canted at low temperature. The spin reorientation in $ErFe_{11.35}Nb_{0.65}$ is actually driven by the six-order term $B_{60}\langle O_{60}\rangle$, which is exceptionally large for Er^{3+} due to its large and positive value

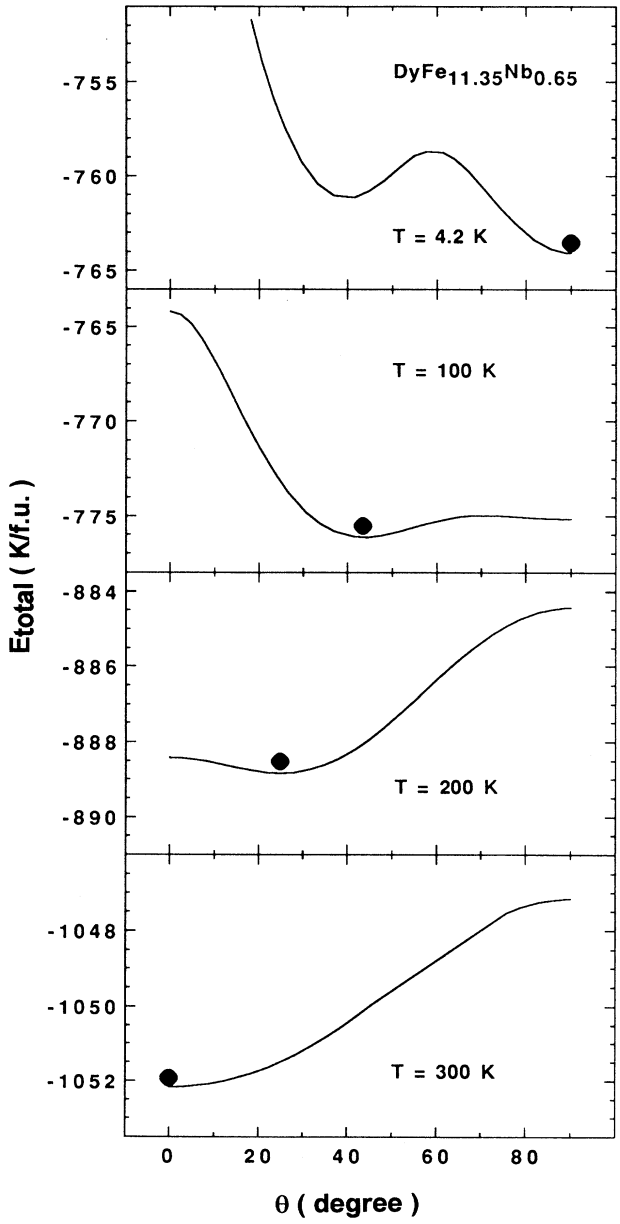

FIG. 17. Calculated energy surfaces in the (010) plane of $DyFe_{11.35}Nb_{0.65}$. The energy minima are θ=90° at 4.2 K, θ=43.5° at 100 K, θ=25.1° at 200 K, and θ=0° at 300 K, shown by black circles.

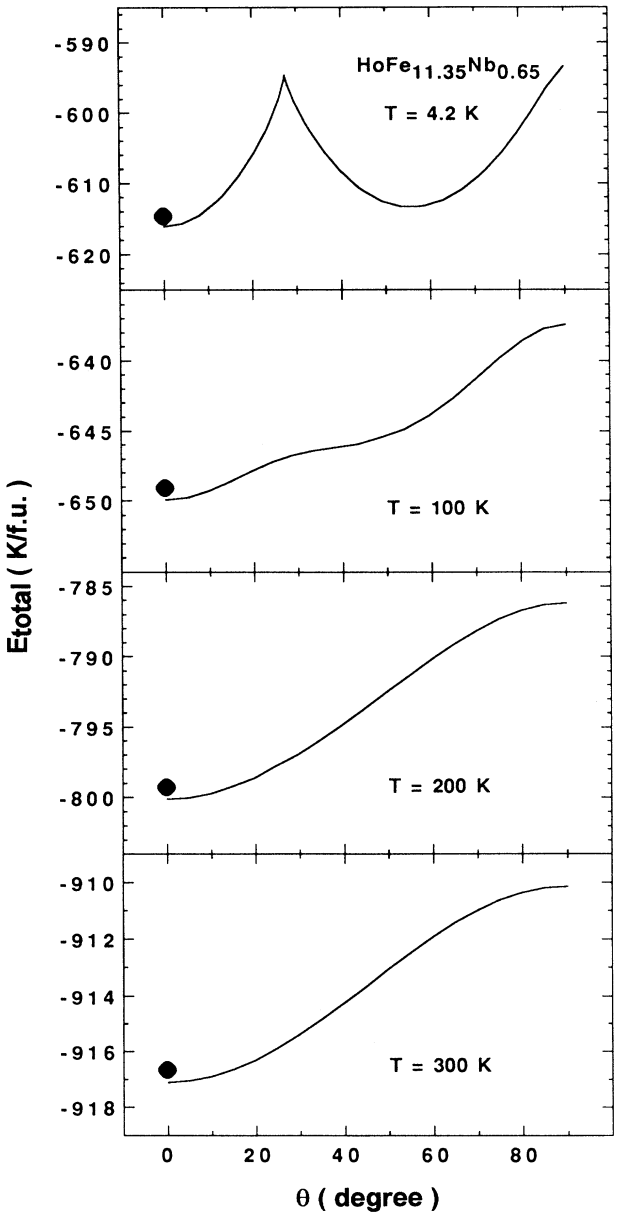

FIG. 18. Calculated energy surfaces in the (010) plane of $HoFe_{11.35}Nb_{0.65}$. The energy minima are 0° at all temperatures, shown by black circles.

of γ_J. The calculated transition temperature $T_{sr}^{calc}=55$ K is close to the experimental value $T_{sr}=41$ K.

Figure 20 shows the predicted temperature variation of θ for $R\mathrm{Fe}_{11.35}\mathrm{Nb}_{0.65}$ (R=Tb, Dy, Ho, and Er). The theoretical calculation is in good agreement with experimental data, except for the Tb compound. The spin-reorientation features in the $R\mathrm{Fe}_{11.35}\mathrm{Nb}_{0.65}$ series are quite similar to those in the $R\mathrm{Fe}_{11}\mathrm{Ti}$.[50] First-order spin-reorientation transitions are present at 168 K for $\mathrm{TbFe}_{11.35}\mathrm{Nb}_{0.65}$ and at 85 K for $\mathrm{DyFe}_{11.35}\mathrm{Nb}_{0.65}$, which are due to the two-minima shape of their total-energy surfaces (see Figs. 16 and 17).

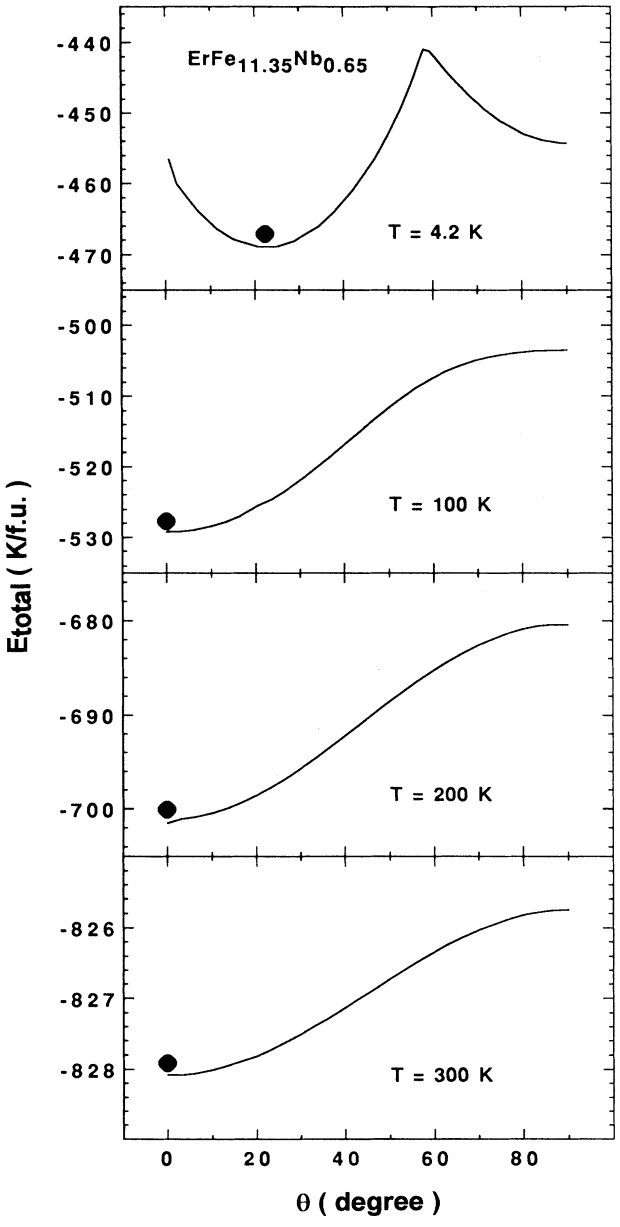

FIG. 19. Calculated energy surfaces in the (110) plane of $\mathrm{ErFe}_{11.35}\mathrm{Nb}_{0.65}$. The energy minima are $\theta=22.5°$ at 4.2 K, $\theta=0°$ at 100 K, $\theta=0°$ at 200 K, and $\theta=0°$ at 300 K, shown by black circles.

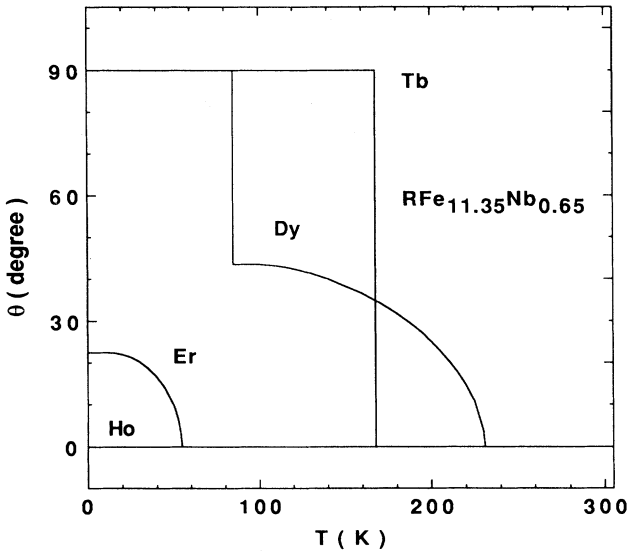

FIG. 20. The calculated temperature variation of the tilting angle θ for $R\mathrm{Fe}_{11.35}\mathrm{Nb}_{0.65}$ (R=Tb,Dy,Ho, and Er).

Other than $\mathrm{TbFe}_{11.35}\mathrm{Nb}_{0.65}$, the other exceptional compound in the $R\mathrm{Fe}_{11.35}\mathrm{Nb}_{0.65}$ series is $\mathrm{SmFe}_{11.35}\mathrm{Nb}_{0.65}$, which is the most interesting one for potential use in permanent magnets due to its large uniaxial anisotropy at room temperature and high Curie temperature. Since the first excited multiplet $^6H_{7/2}$ of Sm^{3+} ion is only 1439 K above the ground state $^6H_{5/2}$ and is much lower than the first excited states of other R^{3+} ions,[56] in order to explain the magnetization of Sm intermetallics it is often necessary to take account of J mixing, such as for $SmCo_5$,[57] $SmFe_{11}Ti$,[58] and $Sm_2Fe_{17}N_y$.[59] The crystal-field interactions in $\mathrm{SmFe}_{11.35}\mathrm{Nb}_{0.65}$ will be discussed elsewhere.

4. *Crystal-field interactions in* $R\mathrm{Fe}_{11.35}\mathrm{Nb}_{0.65}\mathrm{N}_y$

Since the discovery of the nitrides $R_2Fe_{17}N_y$ in 1990,[60,61] the study of interstitial nitrides or carbides has been focused on the 2:17 system[2,45] and the 1:12 system.[4–14] Neutron diffraction showed that the N atoms occupy 9e sites in the Th_2Zn_{17} structure ($y<3$),[62] and 2b sites in the $ThMn_{12}$ structure.[23,24] Since the above two structures come from the same $CaCu_5$ structure,[17] 9e and 2b are from the same original site. Following the model of Coehoorn and co-workers,[63,64] the principal contribution to the electric-field gradient experienced by the 4f shell comes from 5d and 6p electrons of the rare-earth atom itself and the charge density at the boundary of the Wigner-Seitz cell acts as an important factor. The density produced by nitrogen or carbon is particularly large; hence the in-plane configuration of the R-N neighbors found in the 2:17 structures produces a large negative A_{20}, whereas the axial dumbbell found in the 1:12 structure produce a positive A_{20}. At room temperature the second-order crystal-field-interaction term is dominant in determining the R-sublattice anisotropy. So compounds of Sm, Er, Tm, and Yb with $\alpha_J>0$ exhibit uniaxial an-

isotropy when A_{20} is negative, whereas compounds of Ce, Pr, Nd, Tb, Dy, and Ho with $\alpha_J < 0$ exhibit uniaxial anisotropy when A_{20} is positive.

The leading crystal-field parameter A_{20} in $NdFe_{11}TiN_y$ compounds has been determined by Li and Cadogan[48] using the bonding charge model and the exchange- and crystal-field-interaction model. A_{20} increases from -30 K a_0^{-2} for $x=0$ to 370 K a_0^{-2} for $x=1$, with a slope of $dA_{20}/dx = 400$ K a_0^{-2}. The calculated anisotropy field at room temperature is 7.5 T for $NdFe_{11}TiN_{0.5}$ ($A_{20}=170$ K a_0^{-2}) and 13 T for $NdFe_{11}TiN$ ($A_{20}=370$ K a_0^{-2}), compared with the experimental value 8 T for $NdFe_{11}TiN_y$.[7] However, Yang *et al.*[65] derived A_{20} as 85 K a_0^{-2} for the $RFe_{11}TiN_y$ series by crystal-field calculation.

Taking the temperature dependence of the Fe-sublattice magnetization $\mathbf{M}_{Fe}$ and anisotropy constant K_1(Fe) from $YFe_{11.35}Nb_{0.65}N_y$ (see Secs. III C 1 and III C 2), exchange coefficient $n_{RFe}=147\mu_0$ for heavy rare-earth atoms, and $A_{20}=160$ K a_0^{-2}, we calculated the anisotropy field B_a at room temperature for $TbFe_{11.35}Nb_{0.65}N_y$ and $DyFe_{11.35}Nb_{0.65}N_y$, respectively. The values of B_a are 15.0 and 10.5 T for the former and latter, compared with the experimental values of 14.5 and 11.5 T.

IV. CONCLUSION

(1) In rare-earth iron-rich niobium alloys, intermetallic compounds with $ThMn_{12}$-type structure have been discovered, of which a narrow Nb stability region was found to be $0.5 < x < 0.8$ in $GdFe_{12-x}Nb_x$. A smaller amount of $M=$Nb, $x=0.65$, is needed to stabilize the $ThMn_{12}$-structure phase in $RFe_{12-x}Nb_x$ than for the other elements $M=$Ti, V, Cr, Si, etc. Thus a larger magnetization can be realized, together with the large anisotropy and high Curie temperature.

(2) The $RFe_{11.35}Nb_{0.65}$ series exists with $ThMn_{12}$-type structure for the rare-earth elements Sm, Gd, Tb, Dy, Ho, Er, Lu, and Y. The corresponding $RFe_{11.35}Nb_{0.65}N_y$ series synthesized by gas-solid reaction retains the same structure, but with a relative volume expansion of 3%.

(3) Neutron-powder diffraction shows that the Nb atoms occupy 8*i* sites in the $ThMn_{12}$ structure.

(4) The variation of Curie temperatures through the $RFe_{11.35}Nb_{0.65}$ series and their nitrides is typical for rare-earth iron-rich intermetallics, with maxima of 597 and 773 K for $GdFe_{11.35}Nb_{0.65}$ and its nitride, respectively, and minima of 489 and 705 K for $LuFe_{11.35}Nb_{0.65}$ and its nitride, respectively. By introduction of nitrogen, the Fe-Fe exchange interaction is much strengthened while the *R*-Fe exchange interaction is slightly weakened.

(5) The average iron magnetic moment μ_{Fe} at $T=1.5$ K is $1.9\mu_B$ for parent compounds and $2.1\mu_B$ for the nitrides, deduced from $YFe_{11.35}Nb_{0.65}$ and $YFe_{11.35}Nb_{0.65}N_y$, respectively. The enhancement of μ_{Fe} by the influence of interstitial nitrogen is about 11%.

(6) The Fe sublattices of $RFe_{11.35}Nb_{0.65}$ compounds and their nitrides have easy *c*-axis anisotropy in the whole magnetically ordering temperature range. At $T=1.5$ K, the anisotropy constant K_1(Fe) is 25.7 K/f.u. (2.04 MJ m^{-3}) for the parent compounds and 21.9 K/f.u. (1.68 MJ m^{-3}) for the nitrides, also deduced from $YFe_{11.35}Nb_{0.65}$ and $YFe_{11.35}Nb_{0.65}N_y$, respectively. The reduction of K_1(Fe) by the influence of interstitial nitrogen is about 17%.

(7) All the $RFe_{11.35}Nb_{0.65}$ compounds with magnetic rare-earth elements show easy *c*-axis anisotropy at room temperature, except for $R=$Tb. Spin-reorientation transitions were observed in $DyFe_{11.35}Nb_{0.65}$ and $ErFe_{11.35}Nb_{0.65}$ compounds. The complex magnetic behavior at low temperature can be explained by the exchange- and crystal-field-interaction model using a set of crystal-field coefficients $\{A_{nm}\}$ deduced from the magnetization analysis on a $DyFe_{11}Ti$ single crystal.[50]

(8) All the $RFe_{11.35}Nb_{0.65}N_y$ nitrides with magnetic rare-earth atoms show easy *c*-axis anisotropy at room temperature, except for $R=$Sm and Er. The dramatic change of the anisotropy is due to the influence on the rare-earth crystal-field interactions of interstitial nitrogen.

(9) The $SmFe_{11.35}Nb_{0.65}$ compound has an anisotropy field of 10.0 T at room temperature, with a high Curie temperature, and is a potential candidate for applications as a permanent magnet.

ACKNOWLEDGMENTS

We are very grateful to Dr. Hong-Shuo Li for providing us with the program for crystal-field calculation.

[1]Hong-Shuo Li and J. M. D. Coey, in *Handbook of Magnetic Materials*, edited by K. H. J. Buschow (North-Holland, Amsterdam, 1991), Vol. 6, p 1.
[2]K. H. J. Buschow, Rep. Prog. Phys. **549**, 1123 (1991).
[3]M. Jurczky, J. Magn. Magn. Mater. **89**, L5 (1992).
[4]Y. C. Yang, X. D. Zhang, S. L. Ge, Q. Pan, L. S. Kong, H. L. Li, J. L. Yang, B. S. Zhang, Y. F. Ding, and C. T. Ye, J. Appl. Phys. **70**, 6001 (1991).
[5]M. Anagnostou, C. Christides, and D. Niarchos, Solid State Commun. **78**, 681 (1991).
[6]D. P. F. Hurley and J. M. D. Coey, J. Phys. Condens. Matter **4**, 5573 (1992).
[7]Y. C. Yang, X. D. Zhang, L. S. Kong, Q. Pan, and S. L. Ge, Solid State Commun. **78**, 317 (1991).
[8]M. Anagnostou, C. Christides, M. Pissas, and D. Niarchos, J. Appl. Phys. **70**, 6012 (1991).
[9]Y. Z. Wang, G. C. Hadjipanayis, A. Kim, D. J. Sellmyer, and W. B. Yelon, J. Magn. Magn. Mater **104-107**, 1132 (1992).
[10]Y. Z. Wang, B. P. Hu, X. L. Rao, G. C. Liu, L. Yin, W. Y. Lai, W. Gong, and C. G. Hadjipanayis, J. Appl. Phys. **73**, 6251 (1993).
[11]M. Akayama, H. Fujii, K. Yamamoto, and K. Tatami, J. Magn. Magn. Mater. **130**, 99 (1994).
[12]Y. C. Wang, Q. Pan, X. D. Zhang, J. Yang, M. H. Zhang, and

S. L. Ge, Appl. Phys. Lett. **61**, 2723 (1992).
[13]M. Endoh, K. Nakamura, and H. Mikami, IEEE Trans. Magn. **28**, 2560 (1992).
[14]W. Gong and C. G. Hadjipanayis, IEEE Trans. Magn. **28**, 2563 (1992).
[15]H. Sun, M. Akayama, K. Tatami, and H. Fujii, Physica B **183**, 33 (1992).
[16]G. Asti, in *Handbook of Ferromagnetic Materials,* edited by H. J. Buschow and E. P. Wohlfarth (Elsevier, Amsterdam, 1990), Vol. 5, p. 397.
[17]B. P. Hu, H. S. Li, and J. M. D. Coey, J. Appl. Phys. **67**, 4838 (1990).
[18]K. H. J. Buschow and D. B. de Mooij, in *Concerted European Action on Magnets (CEAM),* edited by I. V. Mitchell, J. M. D. Coey, D. Givord, and I. R. Harris (Elsevier, London, 1989), p. 63.
[19]B. P. Hu, Y. Z. Wang, K. Y. Wang, G. C. Liu, and W. Y. Lai (unpublished).
[20]RIETAN is a Rietveld structure analysis program (unpublished). It was adopted from the x-ray Rietveld structure analysis program of F. Izumi, Adv. X-ray Chem. Anal. Jpn. **14**, 43 (1984).
[21]O. Moze, L. Pareti, M. Solzi, and W. I. F. David, Solid State Commun. **66**, 465 (1988).
[22]R. B. Helmholdt and K. H. J. Buschow, J. Less-Common Met. **155**, 15 (1989); R. B. Helmholdt, J. J. M. Vleggaar, and K. H. J. Buschow, *ibid.* **138**, L11 (1988).
[23]Y. Z. Wang, G. C. Hadjipanayis, Z. X. Tang, W. Y. Yelon, V. Papaefthymiou, A. Moukarika, and D. J. Sellmyer, J. Magn. Magn. Mater. **119**, 41 (1993).
[24]H. Sun, Y. Morii, H. Fujii, M. Akayama, and S. Funahashi, Phys. Rev. B **48**, 13 333 (1993).
[25]K. H. J. Buschow, J. Appl. Phys. **63**, 3130 (1988).
[26]B. P. Hu, H. S. Li, J. P. Gavigan, and J. M. D. Coey, J. Phys. Condens. Matter **1**, 755 (1990).
[27]R. Verhoef, F. R. de Boer, Z. D. Zhang, and K. H. J. Buschow, J. Magn. Magn. Mater. **75**, 319 (1988).
[28]J. P. Liu, K. Bakker, F. R. De Boer, T. H. Jacobs, D. B. de Mooij, and K. H. J. Buschow, J. Less-Common Met. **170**, 109 (1991).
[29]B. P. Hu, H. S. Li, H. Sun, and J. M. D. Coey, J. Phys. Condens. Matter **3**, 3983 (1991).
[30]S. S. Jaswal, W. B. Yelon, G. C. Hadjipanayis, Y. Z. Wang, and D. J. Sellmyer, Phys. Rev. Lett. **67**, 644 (1991).
[31]Y. P. Li and J. M. D. Coey, Solid State Commun. **81**, 447 (1992).
[32]Q. N. Qi, Y. P. Li, and J. M. Coey, J. Phys. Condens. Matter **4**, 8209 (1992).
[33]A. R. Williams, V. L. Moruzzi, A. P. Malozemoff, and K. Terakura, IEEE Trans. Magn. **19**, 1983 (1983).
[34]A. P. Malozemoff, A. R. Williams, and V. L. Moruzzi, Phys. Rev. B **29**, 1602 (1984).
[35]J. P. Gavigan, D. Givord, H. S. Li, and J. Voiron, Physica B **149**, 345 (1988).
[36]J. M. D. Coey, J. Magn. Magn. Mater. **80**, 9 (1989).
[37]B. P. Hu, Ph.D. thesis, Trinity College, University of Dublin, 1990.
[38]E. Belorizky, M. A. Fremy, J. P. Gavigan, D. Givord, and H. S. Li, J. Appl. Phys. **61**, 3971 (1987).
[39]K. H. J. Buschow, Rep. Prog. Phys. **40**, 1179 (1977).
[40]E. Burzo, E. Oswold, M. Q. Hung, J. P. Gavigan, D. Givord, and H. S. Li, J. Appl. Phys. **57**, 4109 (1985).
[41]K. Y. Wang, Y. Z. Wang, B. P. Hu, and W. Y. Lai (unpublished).
[42]H. Sun, M. Akayama, and H. Fujii, Phys. Status Solidi A **140**, K107 (1993).
[43]Y. Z. Wang, B. P. Hu, L. Song, K. Y. Wang, and G. C. Liu, J. Phys. Condens. Matter (to be published).
[44]D. P. F. Hurley and J. M. D. Coey, J. Magn. Magn. Mater. **99**, 229 (1991).
[45]H. Sun, Ph.D. thesis, Trinity College, University of Dublin, 1992.
[46]M. S. S. Brooks, O. Eriksson, and B. Johansson, J. Phys. Condens. Mater **1**, 5861 (1989).
[47]H. S. Li, Y. P. Li, and J. M. D. Coey, J. Phys. Condens. Matter **3**, 7277 (1991).
[48]H. S. Li and J. M. Cadogan, J. Magn. Magn. Mater. **109**, L153 (1992).
[49]J. M. Cadogan, J. P. Gavigan, D. Girord, and H. S. Li, J. Phys. F **18**, 779 (1988).
[50]B. P. Hu, H. S. Li, J. M. D. Coey, and J. P. Gavigan, Phys. Rev. B **41**, 2221 (1990).
[51]M. T. Hutchings, *Solid State Physics* (Academic, New York, 1964), Vol. 16, p. 227.
[52]C. Rudowiz, J. Phys. C **18**, 1415 (1985).
[53]H. S. Li, B. P. Hu, and J. M. D. Coey, Solid State Commun. **66**, 133 (1988).
[54]X. C. Kou, T. S. Zhao, R. Grossinger, H. R. Kirchmayr, X. Li, and F. R. de Boer, Phys. Rev. B **47**, 3231 (1993).
[55]C. Christides, D. Niarchos, A. Kostikas, H. S. Li, B. P. Hu, and J. M. D. Coey, Solid State Commun. **72**, 839 (1989).
[56]W. G. Williams, B. C. Boland, Z. A. Bowden, A. D. Taylor, S. Culverhouse, and B. D. Rainford, J. Phys. F **17**, L151 (1987).
[57]S. G. Sankar, V. U. S. Rao, E. Segal, W. E. Wallace, W. G. D. Frederick, and H. J. Garnett, Phys. Rev. B **11**, 435 (1975).
[58]H. S. Li, B. P. Hu, J. P. Gavigan, J. M. D. Coey, L. Pareti, and O. Moze, J. Phys. (Paris) Colloq. **49**, C8-541 (1988).
[59]H. S. Li and J. M. Cadogan, J. Magn. Magn. Mater. **103**, 53 (1992).
[60]J. M. D. Coey and H. Sun, J. Magn. Magn. Mater. **87**, L251 (1990).
[61]H. Sun, J. M. D. Coey, Y. Otani, and D. P. F. Hurley, J. Phys. Condens. Matter **2**, 6465 (1990).
[62]T. Kajitani, Y. Morii, S. Funahashi, T. Iriyama, K. Kobayashi, H. Kato, Y. Nakagawa, and K. Kiraya, J. Appl. Phys. **73**, 6032 (1993).
[63]R. Coehoorn, M. W. Dirken, and K. H. J. Buschow, Phys. Rev. B **42**, 4645 (1990).
[64]R. Coehoorn, J. Magn. Magn. Mater. **99**, 55 (1991).
[65]Y. C. Yang, X. D. Pei, H. L. Li, X. D. Zhang, Li S. Kong, Q. Pan, and M. H. Zhang, J. Appl. Phys. **70**, 6574 (1991).